Research on Running Motion Control of Underactuated Planar Biped Robot

Yang Yang [1, a], Xin Yang [1, b] and Song Liu [1, c]

[1]Automation College, Chongqing University of Posts and Telecommunications, Chongqing 400065, China;

[a]17784236941@163.com, [b]yangxinjob@yeah.net, [c]903433642@qq.com

Abstract

At present, most of the underactuated robots still exist problem in running stability or running speed. For these problems, the paper improves the leg structure of the existing simplest model, increases the telescopic drive and spring model to better adapt to running requirements. it is found that the footing point can adjust the posture balance and running speed during the running movement by analyzing the influence on them. Since the parabola-like trajectory is proved in the running vacant process, the position of the landing point can be controlled by the trajectory prediction method, thereby achieving the speed regulation and posture balance during the running process. In addition, by testing the relationship between the fixed thrust and the single-leg bounce height of the model, it is found that the bounce height is basically stable under the fixed thrust. That is, the height control can be completed by providing a fixed thrust during the support phase of the robot running. Finally, the simulation model of the speed running is realized. The results show that the maximum speed of the two-dimensional running can reach 2.5m/s, and the maximum speed of the three-dimensional running can reach 1.1m/s.

Keywords

Underdrive; Simplest model; Foothold; Running.

1. Introduction

The Leg Laboratory of the Massachusetts Institute of Technology first introduced a series of robots and studied the application of robots to improve the stability and energy efficiency of robots based on passive gait. In the field of running robots, M.Raibert developed the first running 3D robot[1] from 1989 to 1995. Since 1997, the French CNRS and FNRC have jointly developed RABBIT, a point-and-under-actuated planar robot based on time-invariant and feedback control strategies[2]. In 2007, Mabel, a new under-actuated running machine, was developed, and uses a compliant zero-dynamic control strategy to achieve a 3.9 m/s stable running speed, which is by far the fastest biped robot[3]. J.Hurst et al. have developed a highly underactuated 3D robot MARLO since 2012. MARLO has 13 degrees of freedom[4]. It has a similar foot in the bare joint, and has 7 underdrive degrees when the foot is flat. It presents new challenges for underactuated robot control strategies.

Domestic research on running robots has just started, and the main research results are concentrated in Tsinghua University and Peking University. Fu Chenglong of Tsinghua University designed a flat footless semi-passive humanoid robot in 2006 to successfully achieve fast dynamic walking with a walking period of 0.64 and a step length of 0.65 times by studying dynamic walking and bionic control strategies[5]. In 2009, Fu Chenglong introduced the semi-passive underactuated robot THR-II, which uses artificial pneumatic muscle drive and sensory reflection neural control method to achieve a flat walking and stable step with a 0.15m step length and a 0.075m/s pace. Kicking action[6]. This is the

fastest biped robot in China. Zhao Mingguo of Tsinghua University developed the prototype of the compass-type biped robot Stepper2D[7], which realized gait planning and continuous shifting based on the virtual slope walking gait generation algorithm . In 2006, the Intelligent Control Laboratory of Peking University College of Engineering successfully developed a semi-passive humanoid robot Runbo[8] with upper body, which largely simulates human biped walking such as smooth walking and performs tasks such as carts.

In summary, scientists in many countries have done a lot of research on improving the robots performance at present. but compared with humans, there are still shortcomings such as slow speed, low energy efficiency, insufficient flexibility and short duration. As the foot robot can improve its running ability and expand, so its wide use is very necessary. By improving the leg structure of the simplest model, adding telescopic drive and spring model, and controlling the position of the landing point in the robot running process, the 2.5m/s two-dimensional running and the 1.1m/s three-dimensional running of the robot are realized. The running feasibility of the proposed model is verified, which provides theoretical support for the subsequent development of the solid prototype.

2. Biped robot model

By analyzing the running feasibility of the simplest walking model[9], and combining with the motion characteristics of the SLIP model, the telescopic drive and spring model are added to the legs of the simplest walking model, to reduce the impact of collision energy loss on the robot attitude during the running process, and reserve energy for the next vacancy. The basic model is shown in Figure 1.

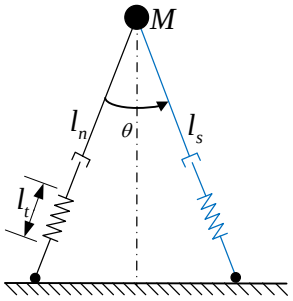

Fig. 1 New running model

3. Derivation of dynamic equations for running model

The motion state of the model is similar to that of the SLIP model, which is mainly divided into the support phase and the flight phase. The kinetic analysis will be carried out for the two stages using the Newton-Euler method and the Lagrange method. In the flight phase, the air resistance is neglected, the robot is only affected by gravity, and the force is relatively simple. The force analysis is performed by Newton's Euler method. The dynamic equation is as follows (here, the model is thrown):

$$\begin{cases} \ddot{z} = -g \\ \ddot{x} = 0 \\ \ddot{\psi} = -\tau / I_l \end{cases} \tag{1}$$

It can be seen from the figure that the robot in the vacant phase has two processes of throwing and falling. The two processes are completely symmetrical, and only the acceleration of gravity is opposite[10]. The formula (1) is a general rule of physical parabolic motion, and the movement of the hip motor drives the leg movement to adjust the position of the robot landing point.

The analysis of the support phase is more complicated than the emptying phase. The whole support phase is from the robot foot contacting the ground to the robot foot leaving the ground. When the robot foot touches the ground, the spring of the leg begins to compress, so the whole system potential energy includes the gravitational potential energy and the spring's elastic potential energy, and the kinetic energy of the system includes the kinetic energy of the robot's rotation, and also includes the spring

telescopic direction motion and the kinetic energy of the robot's forward motion. According to the Lagrangian dynamic equation $L=T-V$, where T is the total kinetic energy of the system and the total potential energy of the V system.

$$\begin{cases} T=\frac{1}{2}m(\dot{l}^2+l^2\dot{\theta}^2)+\frac{1}{2}I_b\dot{\psi}^2+\frac{1}{2}I_l\dot{\theta}^2 \\ V=mg(h+l\cos\theta)+\frac{1}{2}k(l-l_0)^2 \end{cases} \tag{2}$$

The meanings of the variables in the formula are: l represents the length of the current leg, l_0 represents the original length of the leg, θ represents the angle of the leg swing, ψ represents the attitude angle of the model, I_b represents the moment of inertia of the leg, and I_l represents the moment of inertia of the body. , k represents the stiffness coefficient of the leg spring, and h is the height of the sole from the ground. In the selected formula (2), l, θ and ψ are generalized coordinates, then the dynamic equation of the supporting phase is:

$$\begin{cases} \ddot{l}=l\dot{\theta}^2-g\cos\theta-\frac{k(l-l_0)}{m} \\ \ddot{\theta}=-\frac{2\dot{l}\dot{\theta}}{l}+\frac{g\sin\theta}{l}-\frac{I_l\ddot{\theta}^2}{ml^2} \\ \ddot{\psi}=0 \end{cases} \tag{3}$$

4. Spring stiffness coefficient

It can be seen from the literature [11] that the magnitude of the spring stiffness coefficient is determined by the desired support phase support time, and the relationship between them is inversely proportional. The support time can be approximately equal to half of the spring resonance period, and the resonance period can be calculated by the natural frequency of the Spring-mass model, so that the relationship between the natural frequency of the resonance and the stiffness coefficient of the spring can be established[12]. In addition, the maximum value of the spring stiffness coefficient is limited by the time required to limit the attitude adjustment and energy compensation, and the minimum value is limited to the telescopic distance of the telescopic joint. In order to further determine the natural frequency of the model to calculate the stiffness coefficient of the spring, the data of animal jumping and running is obtained by searching relevant data. The data is from the literature [11], and the method of bionics is used to determine the appropriate course of the robot movement. Natural frequency. The team used high-speed cameras to record changes in the natural frequencies of several groups of different masses and different leg lengths during the running and jumping. The literature indicates that the stiffness coefficient of the leg springs is related to the quality. As the mass increases, the bounce The natural frequency will decrease during the process. Using the experimental data in [11] to obtain the relationship between mass and natural frequency, and then fitting the power-finger function curve by MATLAB, the fitting curve is shown in Figure 2, and finally the relationship is as follows：

$$f_n=3.0m^{-0.19}$$

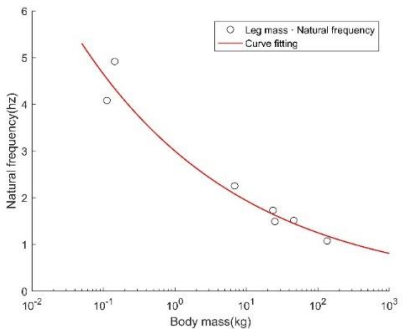

Fig. 2 Two types of relationship curves based on the data from [11]

Substituting the robot model quality parameters into equation $f_n = 3.0m^{-0.19}$, the calculation results are:

$$f_n = 2.28Hz, m = 4.2kg \tag{4}$$

When the natural frequency of the robot movement is too high, the response speed of the robot during the running of the robot is higher. In addition, it also affects the support time during the movement of the robot, shortens the attitude adjustment process of the robot, and increases the difficulty of control. According to the relationship between the natural frequency of the system and the angular velocity,

$$f_n = \frac{1}{2\pi}\omega_n = \frac{1}{2\pi}\left(\frac{k}{m}\right)^{1/2} \tag{5}$$

It can be inferred that the relationship between the stiffness coefficient and the natural frequency is as follows:

$$k = (2\pi f_n)^2 m \tag{6}$$

$k = 861.1N/m$ can be calculated by the above formula. This data provides a reference for the construction of the post-simulation model, and has guiding value for the spring selection of the physical prototype.

5. Robot running motion control

5.1 Forward motion control

The lateral balance of the underactuated planar biped robot studied in this paper is maintained by the symmetry of the mechanism, so the model can be two-dimensionalized in the process of motion control analysis. In addition, according to the characteristics of control during the movement process, the actual control action of the support phase and the vacant phase is only one, both the swing leg and the support leg. In the motion analysis of the upper body, the upper body of the model can also be directly regarded as a quality point. This facilitates the analysis and simplification of the motion process, and the simplified model is the SLIP model. Its motion process can be decomposed into forward speed control and vertical height control. Through the bionic kinematics analysis and the related foreign running sports research, combined with the running test experiment, the forward motion control of the robot running is proposed. The test experiments show that the different landing points of the robot cause different motion trajectories of the robot centroid. The basic track is shown in Figure 3.

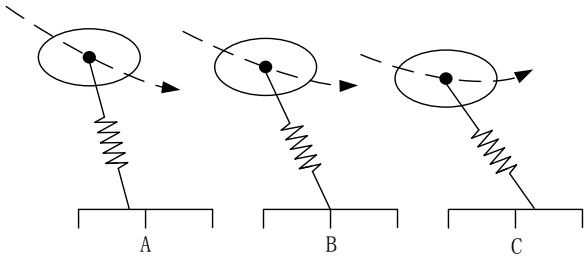

Fig. 3 Robot motion state

It can be seen from the above figure that when the robot's landing point is at the lowest point of its parabolic motion, after the robot is grounded, its motion trajectory is axisymmetric, that is, the motion of the entire centroid from landing to the ground is symmetrical. When the grounding foot falls in front of the symmetrical contact point, its motion trajectory is lower than the normal grounding trajectory, and the robot posture shows a forward tilting state during the movement; when the grounding foot falls behind the symmetrical contact point, the post-touching robot The motion trajectory will be higher than the normal ground motion trajectory, and the robot posture will be tilted backward during the movement.

Through the above analysis and experiments, it is shown that in the support phase, the robot's stationarity control needs to predict the position of the balance point by predicting the motion trajectory of the flight phase, and then adjust the angle of the robot support leg to make it fall near the equilibrium point. Its trajectory is related to the speed of the flight phase, and can be predicted by detecting the speed of the robot's flight phase and the relationship of the object's parabolic motion. In order to solve the problem of balance and speed regulation during the movement of the robot, the control system must calculate the forward position of the foot according to the state of the robot and the desired behavior. The approach taken in this paper is to approximate the position of the equilibrium point by using a rough estimate of the trajectory. The position of the balance point is estimated by the real-time running speed, and the deviation point is adjusted by setting the deviation between the speed and the actual speed. According to the characteristics of the centroid trajectory, when the supporting foot falls in the center position, the angle between the supporting leg and the ground and the position of the body leaning forward are equal to the values at the time of takeoff, but the signs are opposite. The length of the motion trajectory is approximately the product of the forward speed and the duration of the support phase. According to Figure 4, the balance point is half of the distance.

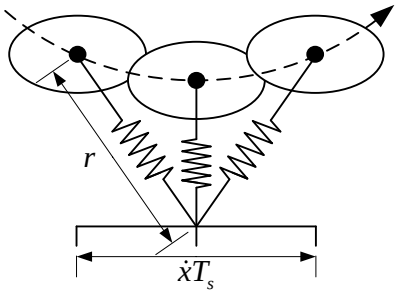

Fig. 4 Balance point calculation track diagram

That is, the following relationship exists:

$$x_{f_0} = \frac{\dot{x}T_s}{2} \tag{7}$$

In the formula, x_{f_0} is the forward displacement of the foot end relative to the center of gravity, $\dot{x}$ is the forward speed and T_s is the duration of the support phase.

Since the oscillation period and amplitude of the spring mass system are independent, the duration of the support phase is almost constant under the condition that the spring coefficient of the spring leg is determined. When calculating the landing point of the next cycle, the last support phase can be used. Time to calculate, so that the robot can run at a constant speed. In order to accelerate the robot, it is necessary to introduce an asymmetrical motion trajectory, that is, to accelerate under stable conditions by appropriately moving the landing point backward. The acceleration method used in this paper adopts the linear function error acceleration relationship. The formula is as follows:

$$x_{f_\Delta} = k_{\dot{x}}(\dot{x} - \dot{x}_d) \tag{8}$$

In the formula, x_{f_Δ} is the displacement of the foot from the equilibrium point, $\dot{x}_d$ is the desired forward speed, and $k_{\dot{x}}$ is the feedback gain.

The formula for calculating the landing point by combining (7) and (8) is:

$$x_f = \frac{\dot{x}T_s}{2} + k_{\dot{x}}(\dot{x} - \dot{x}_d) \tag{9}$$

After calculating the position of the robot's landing point, it needs to be further calculated to obtain the angle θ between the leg and the body, so as to control the hip motor to rotate to reach the specified landing point. The formula for calculating the θ angle is:

$$\theta=\phi-\arcsin(\frac{\dot{x}T_s}{2r}+\frac{k_{\dot{x}}(\dot{x}-\dot{x}_d)}{r}) \tag{10}$$

In addition, the upper body tilt adjustment process needs to be considered, because the angular momentum is conserved during the flight phase, so the inclination of the upper body of the robot during the flight phase is basically fixed, and the inclination adjustment of the upper body can only be performed during the support phase. During the support phase, the friction between the foot and the ground allows the torque generated by the hip motor to act on the upper body, so that the torque can be applied by the hip motor to adjust the upper body posture.

5.2 Running height control

Leg jumping behavior is basically a process of passive oscillation, the details of which are determined by the elasticity of the leg, the mass of the body and the gravity. The entire running process of the robot relies on this passive mechanical oscillation to determine the form of the basic jump motion, and the thrust of the leg during each jump determines the amplitude of the oscillation. In principle, the control system can calculate the thrust by comparing the energy required to reach the ideal jump height with the actual energy, thereby compensating for the difference in leg thrust. However, such calculations need to take into account the kinetic energy of the robot, the elastic energy of the leg springs and the expected energy loss, which is complicated in the actual control process. In this paper, the simpler method is adopted, that is, the control system provides a fixed thrust at each attitude stage to achieve the effect of jumping height balance. Experiments have shown that each fixed thrust value has a unique equilibrium jump height. The greater the thrust, the greater the jump height. The experimental data is shown in Figure 5.

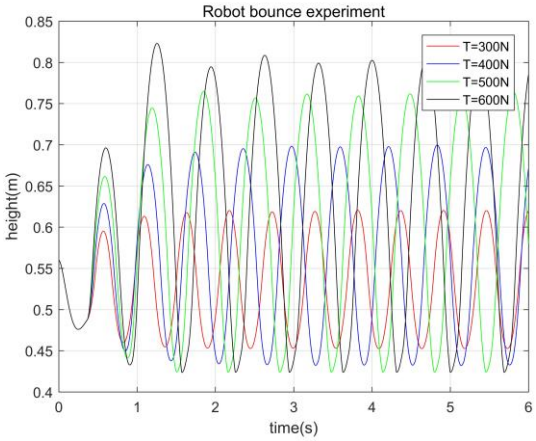

Fig. 5 Leg bounce test data

6. Running control algorithm design

6.1 Motion state machine design

The whole running motion control adopts the state machine mechanism, and the state is switched through relevant conditions. Different states adopt different control strategies to decompose and control the whole system. The entire running process is divided into three state machines: flight state, compression state and extension state. The specific description is as follows:

(1) Flight status mainly realizes the adjustment of the robot's air attitude and the prediction calculation of the foot drop position when the ground is touched, and the support is reached to the corresponding angle through the operation of the hip motor, and the stability of the upper body posture is also required.

(2) Compression state, mainly the natural compression of the spring, through the attitude detection and hip motor to adjust the attitude of the collision and support to prevent the robot from dumping.

(3) Thrust state, after the robot crosses the lowest point, it enters this state. Due to the energy consumption during collision and movement, it is necessary to supplement the energy through the hip motor at this stage.

The actual control further refines it, adding the zero initial state, supporting the initial state, supporting the end state and other intermediate transition states, in order to facilitate the writing of the control amount, so as to avoid a state is too complicated. The state machine control flow chart is shown in Figure 6.

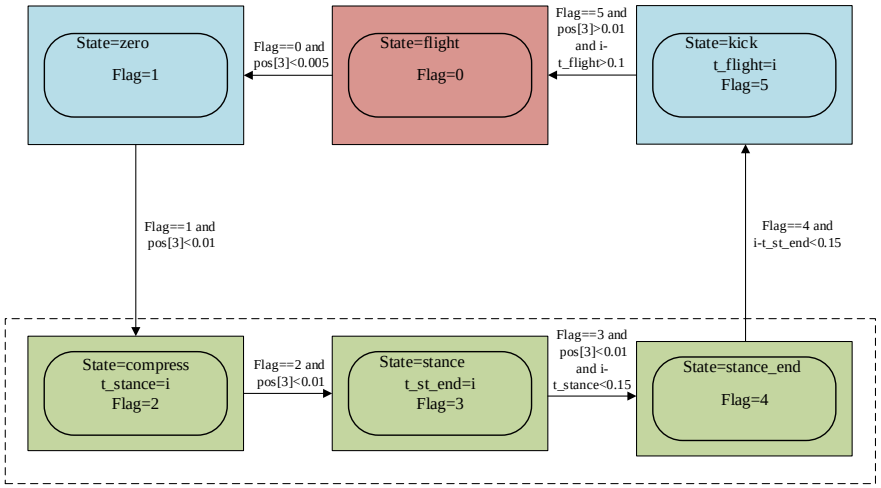

Fig. 6 Running state machine flow chart

6.2 Forward motion controller design

The speed of the robot during the running is to adjust the running speed by controlling the angle of rotation of the hip motor to control the robot's location. Since the simulation environment can't detect the speed of the robot's centroid in the running direction, the running speed is calculated by detecting the moving distance of the robot's centroid along the current running direction. The calculation of the subsequent part is the same as that proposed in the previous theoretical part, and the final calculated angle will be calculated. For the hip motor, the position effect of controlling the robot's location can be achieved, thereby achieving speed control. In addition, the robot attitude angle control compares the set attitude angle with the current attitude angle, and the difference is directly assigned to the angle decision maker. The entire controller is shown in Figure 7.

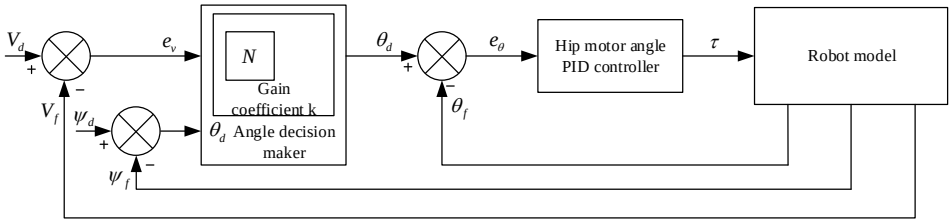

Fig. 7 Running forward motion controller

6.3 Height controller design

Running height control is relatively simple. By applying torque to the robot during the leg extension phase of the robot, the fixed torque applied is 500N according to the bounce height requirement during the actual running process. The bottom motor torque control is performed by changing the current robot state information. The height controller is open loop control, and only the bottom torque control is closed loop control. The bottom torque controller is shown in Figure 8 below.

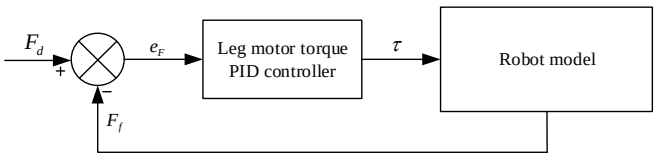

Fig. 8 Running moment bottom torque controller

7. Simulation verification of plane biped robot running algorithm

7.1 Two-dimensional running motion simulation of biped robot with lateral rod

(1) Model establishment and parameter setting

The bipedal robot model with lateral rods is shown in Figure 9. It is mainly composed of laterally balanced spherical joints, fuselage, thighs, calves and foot proximity sensors. The joint between the fuselage and the thigh is connected by a rotating joint. For the hip joint, the elbow and the calf are connected by a telescopic joint, which is called a knee joint. The proximity sensor is mainly used to detect the ground contact during the movement of the robot, and it can detect the straight distance from the sole to the ground in real time.

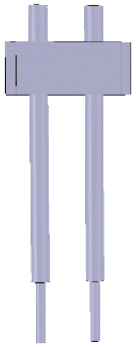

Fig. 9 Two-dimensional running simulation prototype

The overall parameters of the model are shown in Table 1.

Table 1 Two-dimensional Running Simulation Prototype Parameters

Parameter symbol	Parameter meaning	Parameter value
l	Total length of legs	70cm
l_1	Thigh length	55cm
l_2	Calf length	30cm
d	Prototype width	17.5cm
d_o	Leg spacing	10cm
θ	Angle between legs	40°
r	Telescopic distance	10cm
d_{step}	Maximum step size	37.6cm
M_{foot}	Single leg quality	200g
M	Machine quality	3Kg

The V-rep embedded scripting language is used to verify the running algorithm. The knee joint adopts the PD controller for torque control, and then the attitude control algorithm predicts its landing point, controls the robot acceleration and constant speed running, and achieves the highest in the simulation

environment. The 2.5m/s circular running speed can be adjusted by the UI slider. Figure 10 is a simulation screenshot of the robot running motion.

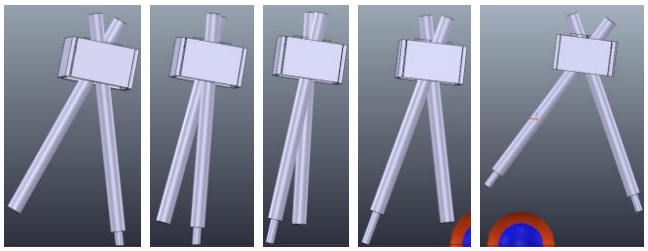

Fig. 10 exploded view of the biped robot with lateral support

(2) Simulation to achieve data analysis

Figure 11 is a graph showing the change of the center of mass height with time during the running movement. Its height has a good periodicity at a constant speed. Combined with the change of the torque of the leg motor in Figure 12, a fixed moment of 500N is applied during the process of extending the leg of the robot. Effective control of the height of the robot during the running process demonstrates the effectiveness of the fixed-torque method for height-direction energy supplementation.

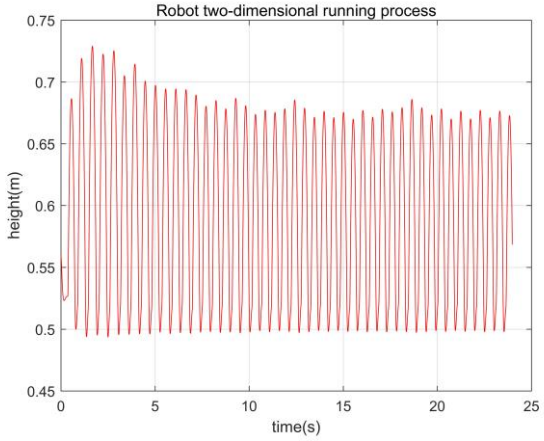

Fig. 11 Two-dimensional running height change

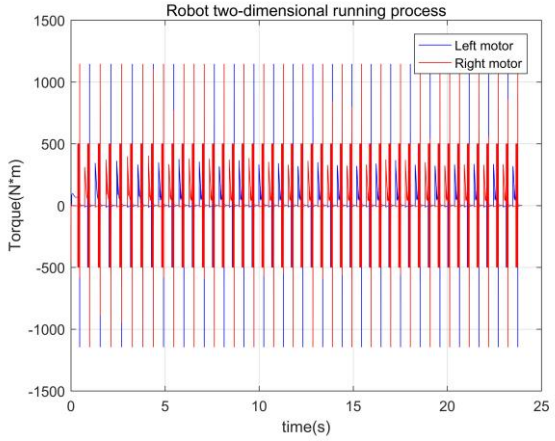

Fig. 12 Two-dimensional running torque change

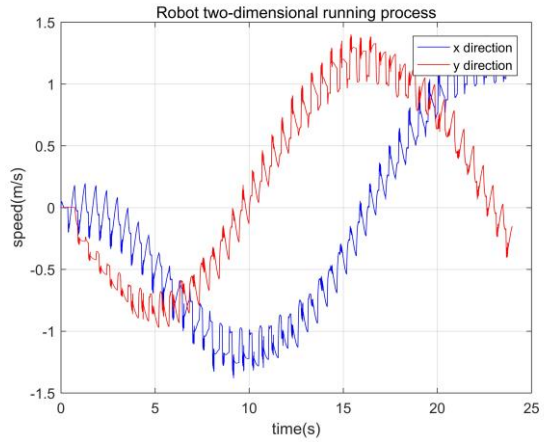

Fig. 13 Two-dimensional running speed change

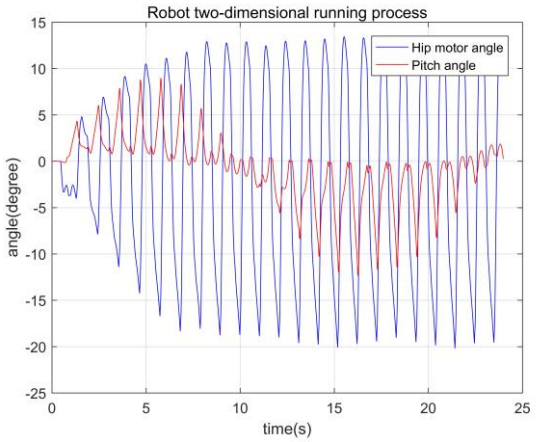

Fig. 14 Two-dimensional running height change

Figure 13 shows the speed change during the running. Since the robot is running in a ring, there will be alternating speeds along the x and y directions. The figure shows the speed of the robot from 0-1.3 m/s, combined with the hip in Figure 14. The change in the angle of the motor reflects the change in the

footing point and demonstrates the effectiveness of the speed control through the position of the landing foot.

7.2 Three-dimensional running motion simulation of planar biped robot

(1) Model establishment and parameter setting

The three-dimensional model built in front is expanded in three dimensions, and the symmetrical design idea is adopted to realize the three-dimensional modeling of the prototype, so that the left and right balance problem in the three-dimensional running process can be effectively solved. The left and right drive mechanisms are synchronously controlled, so as to avoid the instability of the robot during the running process due to the error of the control process during the running process. The simulation prototype is shown in Figure 15.

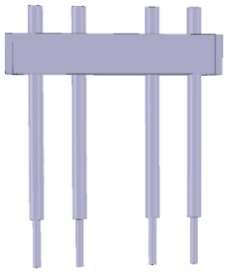

Fig. 15 Plane biped robot prototype speed change

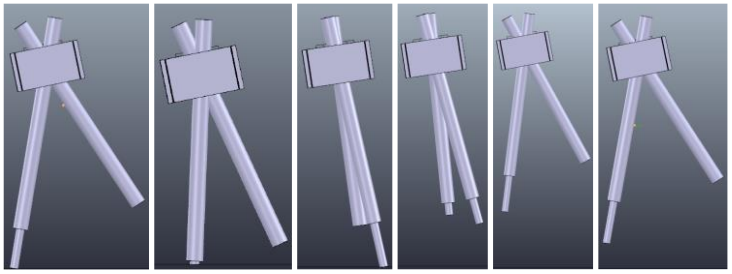

Fig. 16 Three-dimensional running state diagram of planar biped robot

Due to the different physics engines used in the simulation, the robot's motion state is different. For example, in the Vertox engine, the robot can achieve better linear running ability, and its running speed can reach 1.1m/s; in the Newton engine. The robot can achieve a running speed of 2.2m/s, but its running trajectory is a circular running track, which cannot run in a straight line. The main reason is because the Vertox engine has the characteristics of forward and inverse kinematics, and its mechanical characteristics are relatively poor, so the high speed operation is likely to cause the torque to be unstable and the error phenomenon. The Newton engine is just the opposite, so there is a difference in its internal synchronization, which makes the robot prone to yaw during the running. The running states under the Vertox engine are shown in Figure 16.

(2) Simulation to achieve data analysis

The robot running data in the three-dimensional environment is basically the same as the two-dimensional running. The reason is that the simulation is ideal, and the running difference of the symmetric mechanical structure is small. The highest running speed under the Vertox engine is shown in Figure 17. The highest running speed under the Newton engine is shown in Figure 18.

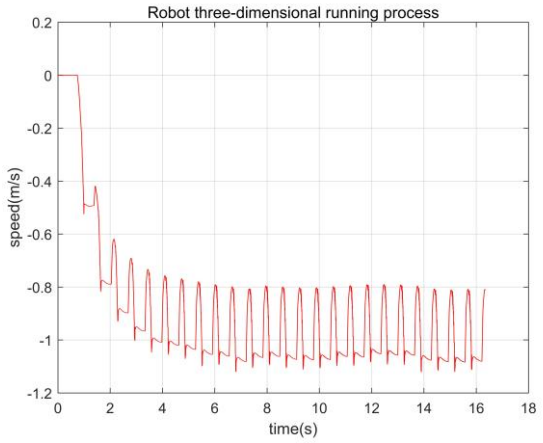

Fig. 17 Three-dimensional running speed change (Vertox)

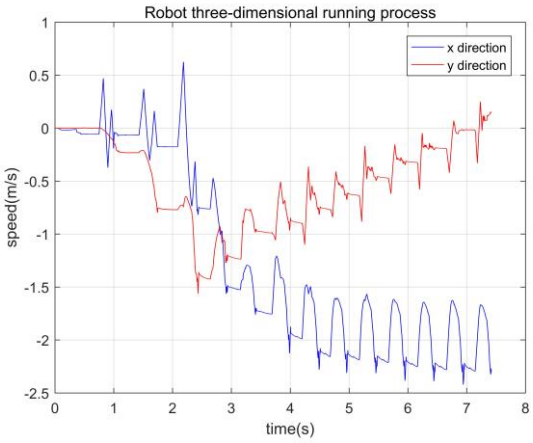

Fig. 18 Three-dimensional running speed change (Newton)

8. Conclusion

In this paper, aiming at the simplest model improvement, we can effectively solve the running problem of the simplest model, and put forward the algorithm of speed and attitude control and height control in the running process of landing point control for the simplest model. The two-dimensional and three-dimensional speed control running in the robot simulation environment is realized. The runnability of the model and the effectiveness of the control algorithm are demonstrated. To a certain extent, the simplest model is expanded. The running ability of the model also provides a solid theoretical basis for the design of the following prototype.

Acknowledgements

Thanks to the laboratory platform and the guidance provided by the instructor.

References

[1] Playter R R, Raibert M H. Control of a Biped Somersault in 3D[C]//Proceedings of the IEEE/RSJ International Conference on Intelligent Robots and Systems. IEEE, 1992, 1: 582-589.
[2] Chevallereau C, Abba G, Aoustin Y, et al. Rabbit: A testbed for advanced control theory[J]. IEEE Control Systems Magazine, 2003, 23(5): 57-79.
[3] Sreenath K, Park H W, Poulakakis I, et al. Design and experimental implementation of a compliant hybrid zero dynamics controller for walking on MABEL[C]//49th IEEE Conference on Decision and Control (CDC). IEEE, 2010: 280-287.
[4] Buss B G, Ramezani A, Hamed K A, et al. Preliminary walking experiments with underactuated 3D bipedal robot MARLO[C]//2014 IEEE/RSJ International Conference on Intelligent Robots and Systems. IEEE, 2014: 2529-2536.
[5] Fu Chenglong, Chen Wei, Wang Jianjian, Huang Yuanlin. Design and Implementation of Dynamic Walking Biped Robot THR-I[J].Robot,2008(02): 123-129.
[6] Fu Chenglong, Huang Yuanlin, Wang Jianjian, Chen Wei. Quasi-open loop control of semi-passive biped robot[J].Robot,2009, 31(02): 110-117+123.
[7] Zhao Mingguo, Dong Hao, Zhang Naiqi. Study on the anti-interference ability of biped robot virtual slope walking[J].Robot, 2010, 32(06): 773-780+786.
[8] Zhai Xiaogang, Qiu Zhongchen, Guan Jialiang. Development Status and Prospect of Biped Walking Robot[J]. Mechanical Engineer, 2007(02): 17-19.
[9] Mcgeer T.Passive Dynamic Walking[J]. The International Journal of Robotics Research, 1990, 9(2):62-82.
[10] Garcia M . The simplest walking model : Stability, complexity and scaling[J]. J. Biomech. Eng. 1998, 120.
[11] Farley C T, Glasheen J, McMahon T A. Running springs: speed and animal size[J]. Journal of experimental Biology, 1993, 185(1): 71-86.
[12] Cavagna G A, Legramandi M A. Running, hopping and trotting: tuning step frequency to the resonant frequency of the bouncing system favors larger animals[J]. Journal of Experimental Biology, 2015, 218(20): 3276-3283.